Microstimulation of primate neocortex targeting striosomes induces negative decision-making

Citation: Amemori, Satoko et al. "Microstimulation of primate neocortex targeting striosomes induces negative decision#making." European Journal of Neuroscience (August 2019): 1-11 © 2019 Federation of European Neuroscience Societies

As Published: https://doi.org/10.1111/ejn.14555

Publisher: Wiley

Persistent URL: https://hdl.handle.net/1721.1/123109

Version: Author's final manuscript: final author's manuscript post peer review, without publisher's formatting or copy editing

Journal section: Behavioral Neuroscience

Title: Microstimulation of primate neocortex targeting striosomes induces negative decision-making

Authors: Satoko Amemori, Ken-ichi Amemori, Tomoko Yoshida, Georgios K. Papageorgiou, Rui Xu, Hideki Shimazu, Robert Desimone, and Ann M. Graybiel*

Affiliations: McGovern Institute for Brain Research and Department of Brain and Cognitive Sciences, Massachusetts Institute of Technology, Cambridge, MA, USA

*Corresponding author:

Ann M. Graybiel

Massachusetts Institute of Technology

43 Vassar Street, 46-6133, Cambridge, MA 02139, United States

E-mail: graybiel@mit.edu

Running title: Cortex targeting striosomes induces negative decision

The number of pages: 29

The number of figures: 3

The number of tables: 1

Total number of words in the whole manuscript: 6834

Total number of words in the Abstract: 248

Keywords: striatum, anterior cingulate cortex, orbitofrontal cortex, microstimulation, approach-avoidance

Abstract

Here we combined MRI-guided electrical microstimulation and viral tracing to examine the function of a corticostriatal circuit implicated by previous cortical microstimulation as modulating affective judgment and decision-making. Local microstimulation of a small part of the pregenual anterior cingulate cortex (pACC) was found to increase avoidance decisions in a cost-benefit decision-making task (Ap-Av task) in which differing amounts of 'good' and 'bad' options were given simultaneously. No effect of such stimulation was found when the monkeys performed a task in which both offers were rewarding, but given in different amounts. We asked whether we could identify the targets of such corticostriatal circuits when the cortical microstimulation sites were explicitly identified as affecting approach or avoidance in the Ap-Av task. We explored the pACC and caudal orbitofrontal cortex (cOFC) to look for such sites. For each cortical region, we found sites at which microstimulation induced increased avoidance behavior. After identifying these sites, we injected viral tracers carrying constructs allowing subsequent track-tracing post-mortem. For each site identified behaviorally as increasing avoidance choices, we found strong fiber projections to the caudate nucleus and anterior striatum with large parts of these targeting striosomes subsequently identified by serial-section immunohistochemistry. With fMRI, we demonstrated that microstimulation in an anaesthetized monkey at sites pre-identified as affecting Ap-Av choices induced BOLD activation of the anterior striatum, confirming that the microstimulation method that we applied was effective in activating the striatum. These findings outline circuits leading from pACC/cOFC to striosomes and causally modulating decision-making under emotional conflict.

1. INTRODUCTION

Microstimulation applied to the neocortex has been of great benefit in examining sensorimotor systems, but applying such methods to cortical regions related to the limbic system and emotion-related performance has been more difficult, both because the behaviors examined are complex and because these cortical regions have not been fully mapped. Few studies have combined microstimulation and behavioral analysis with anatomical output tracing of the stimulated regions. This triple analysis is crucial in order to delineate functional circuits related to affect. Here we developed a method for such triple circuit analysis. We chose to stimulate the pregenual anterior cingulate cortex (pACC), as this region has been shown by microstimulation to affect motivationally challenging cost-benefit decision-making and to project to the striatum (Amemori & Graybiel, 2012; Schmahmann & Pandya, 2006). However, there is no evidence definitively identifying a corticostriatal circuit related to such challenging decision-making, known in humans to be deleteriously affected in neuropsychiatric disorders including anxiety and depression (Pizzagalli, 2011). The presumed rodent homologue of the pACC has been implicated in circuits related to the striosome compartment of the striatum (Banghart *et al.*, 2015; Friedman *et al.*, 2017; Friedman *et al.*, 2015; Yoshizawa *et al.*, 2018), a highly distinct set of labyrinthine zones ('striosomes') distinguished from the surrounding matrix by their neurochemical composition (Graybiel, 1990; Graybiel & Ragsdale, 1978) and connections with the limbic system (Brimblecombe & Cragg, 2017; Fujiyama *et al.*, 2011). Potential homologies between rodent and primate, however, have been questioned, especially for medial prefrontal corticostriatal circuits (Heilbronner *et al.*, 2016). Examining these cortico-striosomal circuits in non-human primates, therefore, has special value (Wise,

2008), as their decision-related circuitry is considered to be more nearly homologous to cortical regions that in humans (Neubert *et al.*, 2015) are implicated in neuropsychiatric disorders (Pizzagalli, 2011).

We have here addressed this need in three ways. First, we applied cortical microstimulation to identify cortical regions that affected cost-benefit decisions in an approach-avoidance (Ap-Av) task used in humans to differentiate anxiety and depression (Amemori & Graybiel, 2012). We combined this with virus-based anatomical identification of the corticostriatal projections of the behaviorally defined cortical regions. In addition, we explored with this behaviorally identified microstimulation-targeting viral tracing to the caudal orbitofrontal cortex (cOFC), which is connected to the pACC and limbic regions and putatively with striosomes in anterior striatum (Eblen & Graybiel, 1995; Schmahmann & Pandya, 2006). Finally, we used fMRI to determine how such cortical microstimulation affected blood oxygen level dependent (BOLD) activity in the striatum to determine whether microstimulation of the behaviorally determined sites indeed activated the striatum. Throughout, we focused on the pACC, known to influence Ap-Av decision-making toward avoidance (Amemori & Graybiel, 2012), and the cOFC, not explored in this task-setting.

2. MATERIALS AND METHODS

2.1. Subjects and experimental conditions

Four female (S: 7.5 kg, P: 6.3 kg, Y: 5.8 kg, A: 6.5 kg) and two male (N: 13.5 kg, I: 13.0 kg) *Macaca mulatta* monkeys were used in microstimulation and/or viral injection experiments. All experimental procedures were approved by the Committee on Animal Care at the Massachusetts Institute of Technology and were in accordance with the

Guide for Care and Use of Laboratory Animals of the United States National Research Council. Before training on behavioral tasks, monkeys S, P and Y were habituated to sitting in a monkey chair and to wearing a head-fixation device (Amemori *et al.*, 2015b). Monkey S was used in neuronal recording, microstimulation and virus injection experiments. Monkey P was used in neuronal recording and microstimulation experiments. Monkey Y was used in microstimulation and virus injection experiments. Monkeys A, N and I were used for anatomy experiments. Monkey N was also used for fMRI imaging with microstimulation. We injected virus tracers in the pACC and/or cOFC of four monkeys (S, Y, A and N). We injected virus tracers in the ventral part of the cingulate motor area of monkey I as control for pACC injections. The details of the procedures that were applied to each monkey are summarized in Table 1.

2.2. Task procedures and microstimulation

Three monkeys (S, P and Y) were trained to perform the approach-avoidance (Ap-Av) task shown in Figure 1a. The task started when the monkey put its hand on the designated position in front of the joystick. After a 1.5-s fixation (precue) period, two bars appeared on the screen as a compound visual cue. The lengths of the red and yellow bars indicated the offered amount of food and airpuff delivered after approach choice, respectively. After the 1.5-s cue period, two targets (cross and square) and an open circle appeared on the screen, and then the monkey could move the circle to choose one of the two targets by the joystick. Cross target was associated with approach (Ap) choice, and the square target was associated with avoidance (Av) choice. The locations of the two targets were randomized across trials. After an Ap decision, both airpuff and reward were delivered as offered. After an Av decision, the monkey did not receive the offered airpuff or food but had a small amount of food to maintain the motivation. When the

monkey made commission or omission errors, the airpuff was delivered at the strength associated with the length of the yellow bar.

After the behavioral training, a plastic recording chamber was implanted on the skull. We used MRI to identify the target region for implanting platinum-iridium electrodes (impedance 1-2 MΩ; FHC, ME) (Figure S1a,b). Single unit activity was also recorded from the cOFC while the monkeys performed the Ap-Av task (Figure S3c). The neuronal recording results for the ACC were published in our previous papers (Amemori *et al.*, 2015a; Amemori & Graybiel, 2012).

During the microstimulation experiment, stimulation-off (*Stim-off*) and stimulation-on (*Stim-on*) blocks were alternated every 200-250 trials. At each trial in the *Stim-on* block, single monopolar stimulation was applied for 1.0 s starting at the onset of cue presentation. The stimulation train consisted of 200-μs pulses delivered at 200 Hz. Each pulse was biphasic and was balanced with the cathodal pulse leading the anodal pulse. The current magnitude was 100-200 μA (Figure 1a). In each microstimulation experiment, we compared the choice pattern in the *Stim-off* and *Stim-on* blocks. For each block, we represented the size of the changes in Ap-Av decision by t-statistics that were calculated from a decision matrix. To make the decision matrix, we first convolved the choice in each trial by 30-by-30 point square-smoothing windows. After the spatial smoothing, each choice datum was stacked at each point in the 100-by-100 decision matrix. We then used two-sided Fisher's exact test to detect statistical differences between the *Stim-off* and *Stim-on* blocks ($P < 0.05$). To calculate the significance level of the difference in decision matrices between the *Stim-off* and *Stim-on* blocks, we measured the total change in decision frequencies as the sum of the increase in Ap and that in Av choices (i.e., $\%\Delta Ap + \%\Delta Av$). We set a change of 5% as the threshold to discriminate effective and non-effective sessions because in our previous study the false-positive rate to misclassify non-effective as effective was less than 5% with the threshold (Amemori *et al.*, 2018) (Figures S2

and S3). After we defined its significance level, we used the difference in positive and negative effects (i.e., %ΔAv − %ΔAp) to clarify the size and direction of each effect. We note that the sum of increases (%ΔAp + %ΔAv) was the same as the difference (%ΔAv − %ΔAp) of the increases in all effective sessions as they exhibited only an increase in Av or Ap for each session.

2.3. Injection of virus tracers into stimulation-effective sites

In order to inject virus tracers into the behaviorally effective site that was identified by microstimulation, we implanted a guide tube that was used in both microstimulation and injection experiments (Figure S1). The guide tube was made with fused silica tubing (TSP250350; outer diameter: 350 μm, inner diameter: 250 μm) and implanted in the pACC of the right hemisphere and the cOFC of both hemispheres in monkey Y. Then we inserted a platinum-iridium electrode (impedance: 3 kΩ; FHC, ME) into the guide tube. The guide tube was held by a small custom-made plastic manipulator for MRI (N0-035-001, Narishige, Japan). The manipulator was attached on top of a custom-made plastic grid that had a hole (outer diameter: 1 mm) at every 1 mm. A guide tube was inserted through each hole. A stopper made from epoxy was attached on top of the electrode to make the tip of the electrode always extend 1-2 mm from the bottom of the guide tube (Figure S1a,b). For the pACC implant, we advanced the guide tube with the electrode by the micromanipulator, targeting the cingulate sulcus. For the cOFC, we implanted the guide tube with the electrode, targeting the white matter above the cOFC. We performed this procedure while taking MRI images of the brain. Thus we could visually confirm the location of the tip of both pACC and cOFC electrodes before starting the first microstimulation experiment. Prior to each microstimulation experiment, we advanced the guide tube holding the electrode ~500 μm, and then the monkey started to

perform the task. If we found a stimulation-effective site, we stopped the guide tube at that site. The electrode tip was again visualized by MRI. Thus we could confirm that the tip of the electrode was below the cingulate sulcus (Figure 1c) and was in the cOFC (Figure 1d) at the effective sites. In monkeys S and Y, after finishing all microstimulation experiments, we removed the electrode but left the guide tube at the effective sites. We measured the length of the electrode and made 32-gauge injection needle that had a stopper exactly at the same position as the electrode in order to inject the virus tracer to the effective sites (Figure S1c,d). The needle was attached to a 10-μl Hamilton syringe (#80008; Hamilton, NV).

2.4. Injection of virus tracers

Monkeys A and I had a craniotomy over the frontal cortex under sevoflurane anesthesia, and a slit was made on the dura. We estimated the target positions for the injection by MRI images as well as the relative position from the midline (for the pACC and the cingulate motor area) and the arcuate sulcus (for the cOFC). After the injection, the slit on the dura was sutured, an artificial dura (DuraGen; IntegraLifeSciences, NJ) was placed to cover the suture, and then the skin was sutured. Monkey N had a craniotomy, and a custom-made chamber was attached over the pACC and cOFC of the right hemisphere (Hong *et al.*, 2019). We estimated the injection position by MRI images and the grid coordination. We used a fused silica guide tube for fMRI in monkey N, and the injection was followed by fMRI.

We used two different virus constructs as neural tracers: AAV-DJ-CMV-hrGFP (genomic titer: 1.10E+14 vg/ml; Infectious titer: 2.50E+09 IU/ml) and AAV-DJ-CMV-mCherry (genomic titer: 2.10E+14 vg/ml; Infectious titer: 3.30E+10 IU/ml;

Stanford Vector Core, CA). The virus tracers and their amount injected are summarized in Table 1. The virus tracer was pressure-injected by a 10-μl Hamilton syringe with a 32-gauge injection needle (#80008, Hamilton, NV). For monkeys A, N and I, after we punched the dura matter by a metal guide tube (27-gauge thin wall stainless steel needle), the needle was advanced to the target position with the control of a stereotactic arm. For monkeys S and Y, we used pre-implanted guide tubes. The injection needle was lowered through the guide tube and stopped at the targeting depth. We injected virus tracers at three different depths along the injection track. Each position was 0.5 mm apart for the pACC and 1 mm apart for the cOFC. The top position was the effective stimulation site in monkeys S and Y, but was estimated in monkeys A, N and I. The injection speed was 0.05 μl/min and was controlled by an injection pump (QSI No. 53311, Stoelting Co., IL). The pump and the syringe were held by a stereotactic arm that was attached on a stereotactic frame. After the injection, the guide tubes were removed immediately except for monkey Y, in which the guide tube was kept in place until perfusion and the virus tracer leaked along the guide tube track. Thus, in monkey Y, the virus was overexpressed above the stimulation effective site in the cOFC, which prevented data analysis. Anti-biotics were given for ten days after the injection for all monkeys. We waited at least seven weeks after the injection to examine the virus expressions in the striatum.

2.5. Histology

We deeply anesthetized the monkeys with an overdose of sodium pentobarbital, and they were perfused with 0.9% saline followed by 4% paraformaldehyde in 0.1 M phosphate buffered saline (PBS). Brains were kept in 4% paraformaldehyde for 3 days,

and then electrodes were withdrawn in monkeys S, P and Y. Brains were kept in 4% paraformaldehyde for only 1 day in monkeys A, N and I. The brains were separated into the left and right hemispheres, and striatal blocks were made. The blocks were stored in 25% glycerol in 0.1% sodium azide (Sigma, 438456) in 0.1 M phosphate buffer (PB) at 4°C until being frozen in dry ice on a sliding microtome and cut into 40-µm coronal sections. Sections were stored in 0.1% sodium azide in 0.1 M PB.

For immunofluorescent staining, sections were rinsed 3 times for 2 min in 0.01 M PBS containing 0.2% Triton X-100 (Tx) (PBS-Tx; Sigma-Aldrich, T8787) and then were pre-treated with 3% H_2O_2 in PBS-Tx for 10 min. Sections were rinsed 3 times for 2 min in PBS-Tx and incubated in tyramide signal amplification (TSA) blocking reagent (PerkinElmer, FP1012) in PBS-Tx (TSA-block) for 60 min. The striatal sections were incubated with primary antibody solutions containing rabbit anti-hrGFP (for hrGFP; 240141, Agilent Technologies) or rabbit anti-RFP (for mCherry; Rockland, 600-401-379) and mouse anti-KChIP1 (UC Davis/NIH Neuro Mab Facility, #75-003) in TSA-block for 24 hrs at 4°C. After primary incubation, the sections were rinsed 3 times for 2 min in PBS-Tx and then incubated for 1 hr in the secondary antibody solution containing goat anti-mouse Alexa Fluor 647 [1:400] (A21236, Invitrogen). After the sections were rinsed 3 times for 2 min in PBS-TX, the sections were incubated in anti-rabbit polymer HRP (GTX83399, GeneTex) solution and then rinsed 3 times for 2 min. The sections were incubated in TSA-block containing Streptavidin 488 [1:2000] (for hrGFP; Jackson Immuno Research, 016-540-084) or Streptavidin 546 [1:2000] (for mCherry; Life Technologies, S11225). We rinsed the sections 3 times for 2 min in 0.1 M PB, mounted onto glass slides and then coverslipped with ProLong Antifade Reagent (Life Technologies, P36930). Sections were examined microscopically, and the striatal regions were imaged with an automatized slide scanner (TissueFAXS Whole Slide Scanner; TissueGnostics, Vienna, Austria) fitted with 10X objectives.

Three fluorescence filter cubes (Alexa 488 for hrGFP, Texas Red for mCherry and Cy5 for KChIP1) were used to image the sections. The images were viewed by TissueFAXS viewer software (TissueGnostics, Vienna, Austria) and exported to tiff images.

2.6. Image analysis

We picked hrGFP/mCherry and KChIP1 images of the same section every ~18 sections (every ~720 μm) from the start to the end of the striatum. Striosome and matrix masks were generated from the KChIP1 image by k-mean clustering function of Matlab (Mathworks, MA), which separated the image into three clusters (striosome, matrix and background) based on the darkness of the image. The hrGFP/mCherry image was transformed into grayscale. In each image, the density of gray value (0-255) per pixel in striosomes and matrix was calculated using the striosome and matrix masks. The density was statistically compared between striosomes and matrix by two-sided paired sample *t*-test in each anterior, central and posterior region (Figures S7-S9). To combine the data from all monkeys, we calculated the normalized gray value in which the density was normalized by the mean density of both striosomes and matrix from both hemispheres in each monkey. The normalized gray value was statistically compared between striosomes and matrix by two-sided paired sample *t*-test in each aterior, central and posterior regions (Figures 2 and 3). In this study, the anterior-posterior (AP) position in millimeters was determined according to the monkey brain atras by Paxinos et al. (2000).

2.7. Detecting corticostriatal pathways in fMRI

Monkey N underwent electrical microstimulation (EM) and fMRI under anesthesia inside a 3T MRI scanner (Siemens, Erlangen, Germany) using a saddle-shaped single-loop 12.7-cm receive coil. During the initial anesthesia by ketamine (1 mg/kg), we implanted a fused silica guide tube

and inserted a tungsten electrode (impedance: 1-3 kΩ; FHC, ME) through the guide tube to the pACC and cOFC. The grid coordination and target sites for the EM-fMRI were the same as those for the injections and confirmed by MRI before starting the EM-fMRI sessions. We maintained anesthesia by continuous intravenous administration of propofol (3-4 mg/kg), at an infusion rate of 0.1-0.6 mg/kg/min. Respiratory rate was assessed by continuous capnographic evaluation, and the body temperature of the animal was kept constant throughout the procedure by heated water blankets and was monitored at the intervals between scans. Probes for measuring blood oxygenation and heart rate were attached, and these measures were recorded continuously. Before starting functional scans, Ferumoxytol (Feraheme), an iron oxide-based contrast agent, was administered intravenously (8 mg/kg), which substantially increases the signal-to-noise ratio of fMRI (Leite *et al.*, 2002). The scanning session lasted ~4 hrs in total.

During the session, four functional runs of EM-fMRI were performed for each region of interest (ROI), using a standard block design and parameters of microstimulation similar to previous studies in this field (Ekstrom *et al.*, 2008; Matsui *et al.*, 2011; Moeller *et al.*, 2008). Specifically, each functional run included eight 30-s EM blocks interleaved with nine 30-s rest blocks in which no stimulation was delivered. During EM blocks, 210-ms pulse trains were delivered at a rate of 1 Hz, which consisted of 70 biphasic current pulses. A single pulse was composed of a 200-μs negative phase, a 100-μs interval, and a 200-μs positive phase. Inter-pulse interval was set at 2.5 ms so that the frequency of microstimulation was 333 Hz. The amplitude of both negative and positive phases was set at 500 μA (Matsui *et al.*, 2011), because we found (data not shown) that this parameter provides a superior contrast-to-noise ratio of EM-fMRI compared to lower current levels (e.g., 300 μA or lower), which given our scanning parameters might render some EM-fMRI activations difficult to detect. Stimulation pulses were delivered in a monopolar configuration with a computer-triggered pulse generator (DS8000;

World Precision Instruments) connected to an isolator (A365; World Precision Instruments). The triggering of pulses was controlled and synchronized with MRI data collection using a desktop computer and custom Matlab code based on Psychtoolbox. Both stimulation and reference electrodes were connected to the isolator through custom-made inductor-based low-pass filters both on the patch-panel and inside the bore of the magnet of the scanner room to avoid contamination of the MR images as well as excessive heat from radio frequency noise.

MRI data were analyzed with Freesurfer/FsFast. A high-quality T1-weighted image collected before the EM-fMRI session was used as a template, and the functional data were co-registered to this template in a two-step fashion, using the T1-weighted image collected during the EM-fMRI session as an intermediate template (same session). Besides common processing steps including slice-timing correction and motion correction, field maps collected close to the functional images (between which there was little movement of the animal) were used to correct geometric distortion of functional data and thus improve its alignment with same-session T1 template. EM-fMRI activation maps (t-score) were computed in the native functional voxel space using FsFast's generalized linear model implementation for each ROI separately and were interpolated to the high-quality T1 template for visualization.

3. RESULTS

Three monkeys, S, Y and P, learned to perform the Ap-Av decision-making task (Amemori & Graybiel, 2012) (Figure 1a; Materials and Methods). After viewing combined stimuli indicating relative amounts of reward (juice) and punishment (airpuff to face), the monkeys indicated their choices by joystick movements to accept or reject the offer. Guided by MRI, we lowered electrodes to circumscribed locations in the pACC and cOFC to test whether microstimulation induced a significant change in the

decision-making patterns (Figure S1a-c). We examined the effects of focal microstimulation (200-μs pulses delivered at 200 Hz, 100-200 μA) applied at 43 pACC and 35 cOFC sites during the first 1.0 s of the 1.5 s cue period. We compared the decision-making patterns between blocks of trials without stimulation (*Stim-off* block of 150-250 trials) and those with stimulation (*Stim-on* block of 150-250 trials; Materials and Methods).

We compared the sizes of changes in decision induced by the microstimulation in the ventral bank of the anterior cingulate sulcus (pACC) to those in the dorsal sulcal bank (dACC) in monkeys S, Y and P. We binned those stimulation effects for every 1 mm from the cingulate sulcus and found that the size of increase in Av induced by the pACC stimulation 1 mm below the sulcus was significantly greater than that induced by the dACC stimulation (two-sided signed rank test, $P < 0.001$) (Figures 1b,c and S2), confirming our previous evidence (Amemori & Graybiel, 2012). In the cOFC of monkeys Y and P, we compared microstimulation effects between white and gray matter by binning the effects for every 1 mm from the gray matter border, and found two cOFC sites at which the microstimulation induced significant increase in Av choices compared to those in the dorsally adjoining white matter (signed rank test, $P < 0.05$) (Figures 1b,d and S3). These effects in the cOFC have not been reported before, and suggest a second cortical source of negative bias in decision-making.

To examine whether stimulation of the pACC and cOFC actually induced striatal activation, we delivered microstimulation in monkey N (anesthetized) during periods in which we performed fMRI imaging (Matsui *et al.*, 2011; Tolias *et al.*, 2005) (Materials and Methods), targeting the microstimulation at the cOFC region corresponding to the locations at which stimulation increased avoidance in monkeys S, Y and P. Control

dACC microstimulation did not induce significant striatal BOLD activation, whereas the targeted pACC stimulation activated the striatum bilaterally. In the cOFC, microstimulation primarily activated striatal regions ipsilateral to the stimulation sites (Figures 1c,d and S4). Thus stimulation of the behaviorally effective sites, but not nearby sites in the pACC and cOFC, indeed activated the striatum.

We next injected viral tracers (AAVDJ-CMV-hrGFP or AAVDJ-CMV-mCherry) at these behaviorally identified pACC and cOFC sites (Table 1; Figures 2c, 3c and S1d-f; Materials and Methods). Seven weeks later, we performed dual immunostaining of corticostriatal afferents for hrGFP or mCherry antibody (virus tracer) and KChIP1 (striosome marker) on the same striatal sections. For the pACC, the injection sites in monkeys S and Y were pre-identified by the stimulation results of the monkeys, and the virus-infected regions around the injection sites of monkeys A and N were confirmed to include the locations of stimulation-effective sites in the post-mortem examination (Figure 2c). Behaviorally effective microstimulation sites in the pACC exhibited preferential targeting of subsets of striosomes, mainly in the anterior striatum (Figures 2a and S5). For the cOFC, we predetermined the injection sites of monkeys A and N by the effective sites of the microstimulation experiments performed in monkeys Y and P, and we confirmed histologically that the infected regions around the injection sites included the locations of the effective sites (Figure 3c). Injections at effective stimulation sites in the cOFC led to labeling of striosomes in ventral regions of the anterior striatum (Figures 3a and S6). Thus there was a significant striosomal bias in corticostriatal projections from the pACC and cOFC sites inducing increased avoidant behavior.

We quantitatively estimated for the sites producing increased avoidance the virally labeled zones in the striosomes and matrix in extensive anterior, central and

posterior striatal regions (Figures 2b, 3b, S7 and S8; Materials and Methods). The densities were significantly higher in striosomes than in matrix (paired t-test, $P < 0.05$ for ipsilateral striatum), suggesting that pACC and cOFC sites at which microstimulation could alter conflict decision-making both provided relatively concentrated striatal input to striosomes. As is commonly found, even concentrated projection zones are accompanied by weaker staining beyond their borders (Eblen & Graybiel, 1995). That was the case here. As a further control, we therefore injected AAVDJ-CMV-mCherry (Table 1) into the caudal ventral cingulate motor area in monkey I, posterior to the effective pACC zone. The matrix compartment, but not striosomes, was mainly labeled (Figure S9). These results indicated a decline of the striosome-projecting cingulate cortex posterior to the pACC, and suggest that only a limited region of the cingulate cortex sends signals to the anterior striosomal system.

4. DISCUSSION

These findings are the first to demonstrate that cortical sites in non-human primates behaviorally identified as modulating conflict decision-making send corticostriatal innervations favoring the striosome compartment over the surrounding matrix. The sites at which microstimulation increased avoidance preferentially targeted striosomes in each monkey, in at least some topographically distinct innervation zone. Our results in non-human primates provide causal evidence that circumscribed, behaviorally identified zones in the pACC and cOFC participate in corticostriatal circuits that contribute critically to negative decision-making under challenging cost-benefit decision-making.

This study was subject to limitations, some of which we mention here. First, it is highly likely that the cortical regions (the pACC and cOFC) preferentially targeting

striosomes are not the only cortical regions that innervate striosomes, and certainly that these pACC and cOFC regions represent only a limited representation of corticostriatal or other corticofugal circuits that impact emotional decision-making. For example, Saga et al. found that microstimulation of the anterior insula induced disturbance of the approach-avoidance behavior (Saga *et al.*, 2019). The pACC and the cOFC are interconnected with the amygdala (Ghashghaei *et al.*, 2007), and with other limbic regions, which could also be sources of the behavioral effects observed. Further, the identified pACC and cOFC regions are likely not the only cortical regions that send projections to striosomes; and even in the pACC and cOFC, we did not fully cover the sites likely to send signals to striosomes in the anterior striatum (Eblen & Graybiel, 1995), We did, however, show the caudal part of the ventral cingulate cortex, likely to be within the cingulate motor area, projects preferentially to the matrix compartment of the striatum (Figure S9). This result suggests that there is likely a caudal border or gradient beyond which the corticostriatal targeting of striosomes declines. Further studies are needed to identify the neocortex projecting to striosomes in more caudal parts of the striatum than those we examined here, and to identify regions with corticostriatal input differentially recruited in approach choices, or both approach and avoidance (Kolling *et al.*, 2016).

Differential effects of neurodegenerative disorders on striosomes and matrix have been indicated by post-mortem studies in humans (Goto *et al.*, 2005; Jarrett *et al.*, 2018; Tippett *et al.*, 2007). The identification here of behaviorally identified cortical sites with differential striosome-matrix connectivity could help to unravel the circuit-level basis affected in such clinical disorders.

ACKNOWLEDGEMENTS

We thank Drs. Helen Schwerdt, Simon Hong, Leif Gibb and Patrick Tierney for help with experiments; Margo Cantor, Jonathan Gill, Caitlin Erickson, Lauren Stanwicks, Alexandra Burgess and Polly Weigand for help with monkey care and training; Jannifer Lee, Michael Riad, Drs. Christian Wuethrich and Thomas Diefenbach for help with histology and imaging; Hanna May, Zahra Malik and Emily Chung for help with histology and image analysis; Henry Hall and Dr. Dan Hu for help with many aspects of this work; and Dr. Yasuo Kubota and Sarah Ryan for help with manuscript preparation. We thank Athinoula A. Martinos Imaging Center at the McGovern Institute for Brain Research, MIT for use of MRI; and Imaging Core at the Ragon Institute of MGH, MIT, and Harvard for use of TissueFAXS scanner. This research was supported by the National Institutes of Health (R01 NS025529), the CHDI Foundation (A-5552), the Office of Naval Research (N00014-07-1-0903), the Army Research Office (W911NF-16-1-0474), MEXT KAKENHI (18H04943 and 18H05131), the Simons Center for the Social Brain, the Saks Kavanaugh Foundation, the Naito Foundation, the Uehara Foundation, P. Dana Bartlett, Amy Sommer, and Judy Goldberg.

CONFLICT OF INTEREST

The authors declare no conflict of interests.

DATA ACCESSIBILITY

The data generated and analyzed and codes used in this study are available from the corresponding author on reasonable request.

AUTHOR CONTRIBUTIONS

S.A., K.A., and A.M.G. designed the experiments. S.A., K.A., H.S. and A.M.G. performed the surgeries and injection experiments. S.A. and K.A. collected the recording and stimulation data and analyzed the electrophysiological data with critical feedbacks from A.M.G. S.A., T.Y. and A.M.G. performed histology and analyzed the anatomical data. S.A., G.P., R.X. and R.D. performed fMRI experiment, and G.P. analyzed the fMRI data. S.A., K.A. and A.M.G. wrote the manuscript.

ABBREVIATIONS

ACC, anterior cingulate cortex; AP, anterior-posterior; Ap, approach; Av, avoidance; BOLD, blood oxygen level dependent; cOFC, caudal orbitofrontal cortex; dACC, dorsal sulcal bank of the anterior cingulate cortex; EM, electrical microstimulation; hrGFP, humanized renilla reniformis green fluorescent protein; HRP, horseradish peroxidase; KChIP1, Kv channel-interacting protein 1; MR, magnetic resonance; pACC, pregenual anterior cingulate cortex; PB, phosphate buffer; PBS, phosphate buffered saline; PBS-TX, PBS containing 0.2% Triton X-100; RFP, red fluorescent protein; ROI, region of interest; SEM, standard error of mean; Stim, stimulation; TSA, tyramide signal amplification.

REFERENCES

Amemori, K., Amemori, S., & Graybiel, A.M. (2015a). Motivation and affective judgments differentially recruit neurons in the primate dorsolateral prefrontal and anterior cingulate cortex. *Journal of Neuroscience*, *35*, 1939-1953.

Amemori, K., & Graybiel, A.M. (2012). Localized microstimulation of primate pregenual cingulate cortex induces negative decision-making. *Nature Neuroscience*, *15*, 776-785.

Amemori, K.I., Amemori, S., Gibson, D.J., & Graybiel, A.M. (2018). Striatal Microstimulation Induces Persistent and Repetitive Negative Decision-Making Predicted by Striatal Beta-Band Oscillation. *Neuron*, *99*, 829-841 e826.

Amemori, S., Amemori, K., Cantor, M.L., & Graybiel, A.M. (2015b). A non-invasive head-holding device for chronic neural recordings in awake behaving monkeys. *Journal of Neuroscience Methods*, *240*, 154-160.

Banghart, M.R., Neufeld, S.Q., Wong, N.C., & Sabatini, B.L. (2015). Enkephalin disinhibits mu opioid receptor-rich striatal patches via delta opioid receptors. *Neuron*, *88*, 1227-1239.

Brimblecombe, K.R., & Cragg, S.J. (2017). The striosome and matrix compartments of the striatum: A path through the labyrinth from neurochemistry toward function. *ACS Chemical Neuroscience*, *8*, 235-242.

Eblen, F., & Graybiel, A.M. (1995). Highly restricted origin of prefrontal cortical inputs to striosomes in the macaque monkey. *Journal of Neuroscience*, *15*, 5999-6013.

Ekstrom, L.B., Roelfsema, P.R., Arsenault, J.T., Bonmassar, G., & Vanduffel, W. (2008). Bottom-up dependent gating of frontal signals in early visual cortex. *Science*, *321*, 414-417.

Friedman, A., Homma, D., Bloem, B., Gibb, L.G., Amemori, K.I., Hu, D., Delcasso, S., Truong, T.F., Yang, J., Hood, A.S., Mikofalvy, K.A., Beck, D.W., Nguyen, N., Nelson, E.D., Toro Arana, S.E., Vorder Bruegge, R.H., Goosens, K.A., & Graybiel, A.M. (2017). Chronic stress alters striosome-circuit dynamics, leading to aberrant decision-making. *Cell*, *171*, 1191-1205 e1128.

Friedman, A., Homma, D., Gibb, L.G., Amemori, K., Rubin, S.J., Hood, A.S., Riad, M.H., & Graybiel, A.M. (2015). A corticostriatal path targeting striosomes controls decision-making under conflict. *Cell*, *161*, 1320-1333.

Fujiyama, F., Sohn, J., Nakano, T., Furuta, T., Nakamura, K.C., Matsuda, W., & Kaneko, T. (2011). Exclusive and common targets of neostriatofugal projections of rat striosome neurons: a single neuron-tracing study using a viral vector. *European Journal of Neuroscience*, *33*, 668-677.

Ghashghaei, H.T., Hilgetag, C.C., & Barbas, H. (2007). Sequence of information processing for emotions based on the anatomic dialogue between prefrontal cortex and amygdala. *Neuroimage*, *34*, 905-923.

Goto, S., Lee, L.V., Munoz, E.L., Tooyama, I., Tamiya, G., Makino, S., Ando, S., Dantes, M.B., Yamada, K., Matsumoto, S., Shimazu, H., Kuratsu, J., Hirano, A., & Kaji, R. (2005). Functional anatomy of the basal ganglia in X-linked recessive dystonia-parkinsonism. *Annals of Neurollogy*, *58*, 7-17.

Graybiel, A.M. (1990). Neurotransmitters and neuromodulators in the basal ganglia. *Trends in Neuroscience*, *13*, 244-254.

Graybiel, A.M., & Ragsdale, C.W., Jr. (1978). Histochemically distinct compartments in the striatum of human, monkey, and cat demonstrated by acetylthiocholinesterase staining. *Proceedings of the National Academy of Sciences of the United States of America*, *75*, 5723-5726.

Heilbronner, S.R., Rodriguez-Romaguera, J., Quirk, G.J., Groenewegen, H.J., & Haber, S.N. (2016). Circuit-Based Corticostriatal Homologies Between Rat and Primate. *Biologial Psychiatry*, *80*, 509-521.

Hong, S., Amemori, S., Chung, E., Gibson, D.J., Amemori, K.I., & Graybiel, A.M. (2019). Predominant Striatal Input to the Lateral Habenula in Macaques Comes from Striosomes. *Current Biology*, *29*, 51-61 e55.

Jarrett, P., Easton, A., Rockwood, K., Dyack, S., McCollum, A., Siu, V., Mirsattari, S.M., Massot-Tarrus, A., Beis, M.J., D'Souza, N., & Darvesh, S. (2018). Evidence for Cholinergic Dysfunction in Autosomal Dominant Kufs Disease. *Canadian Journal of Neurollogical Sciences*, *45*, 150-157.

Kolling, N., Behrens, T., Wittmann, M.K., & Rushworth, M. (2016). Multiple signals in anterior cingulate cortex. *Currrent Opinion in Neurobiology*, *37*, 36-43.

Leite, F.P., Tsao, D., Vanduffel, W., Fize, D., Sasaki, Y., Wald, L.L., Dale, A.M., Kwong, K.K., Orban, G.A., Rosen, B.R., Tootell, R.B., & Mandeville, J.B. (2002). Repeated fMRI using iron oxide contrast agent in awake, behaving macaques at 3 Tesla. *Neuroimage*, *16*, 283-294.

Matsui, T., Tamura, K., Koyano, K.W., Takeuchi, D., Adachi, Y., Osada, T., & Miyashita, Y. (2011). Direct comparison of spontaneous functional connectivity and effective connectivity measured by intracortical microstimulation: an fMRI study in macaque monkeys. *Cerebral Cortex*, *21*, 2348-2356.

Moeller, S., Freiwald, W.A., & Tsao, D.Y. (2008). Patches with links: a unified system for processing faces in the macaque temporal lobe. *Science*, *320*, 1355-1359.

Neubert, F.X., Mars, R.B., Sallet, J., & Rushworth, M.F. (2015). Connectivity reveals relationship of brain areas for reward-guided learning and decision making in human and monkey frontal cortex. *Proceedings of the National Academy of Sciences of the United States of America*, *112*, E2695-2704.

Paxinos, G., Huang, X.-F., & Toga, A.W. (2000). *The Rhesus Monkey Brain in Stereotaxic Coordinates*. Academic Press, San Diego.

Pizzagalli, D.A. (2011). Frontocingulate dysfunction in depression: toward biomarkers of treatment response. *Neuropsychopharmacology*, *36*, 183-206.

Saga, Y., Ruff, C.C., & Tremblay, L. (2019). Disturbance of approach-avoidance behaviors in non-human primates by stimulation of the limbic territories of basal ganglia and anterior insula. *Eurpean Journal of Neuroscience*, *49*, 687-700.

Schmahmann, J., & Pandya, D. (2006). *Fiber Pathways of the Brain*. Oxford University Press.

Tippett, L.J., Waldvogel, H.J., Thomas, S.J., Hogg, V.M., van Roon-Mom, W., Synek, B.J., Graybiel, A.M., & Faull, R.L.M. (2007). Striosomes and mood dysfunction in Huntington's disease. *Brain*, *130*, 206-221.

Tolias, A.S., Sultan, F., Augath, M., Oeltermann, A., Tehovnik, E.J., Schiller, P.H., & Logothetis, N.K. (2005). Mapping cortical activity elicited with electrical microstimulation using FMRI in the macaque. *Neuron*, *48*, 901-911.

Wise, S.P. (2008). Forward frontal fields: phylogeny and fundamental function. *Trends in Neuroscience*, *31*, 599-608.

Yoshizawa, T., Ito, M., & Doya, K. (2018). Reward-predictive neural activities in striatal striosome compartments. *eNeuro*, *5*, e0367-0317.2018.

FIGURE CAPTIONS

FIGURE 1. Task and Behavior. (a) Approach-avoidance (Ap-Av) task (see Materials and Methods). (b) Example of decision pattern affected by pACC (top) and cOFC (bottom) microstimulation, illustrated by choice: before (*Stim-off*, left) and during (*Stim-on*, middle) stimulation (*Stim-off*, left), and smoothed decision difference between the two blocks (right, *t*-statistics). Dashed and solid lines indicate decision boundary. (c) pACC microstimulation increased Av choices compared to dACC stimulation (Wilcoxon signed rank test, ***P = 0.000053). Left: Size of increase in Av subtracted by that in Ap (black cross: %ΔAv − %ΔAp) plotted for the depth from cingulate sulcus. Gray, dACC. Yellow, pACC. Red star, experiment in b. Red lines, mean. Pink bars, standard errors of the means (SEM). Middle: Striatal fMRI signal induced by dACC (top) and pACC (bottom) stimulation in monkey N. BOLD signal intensity over threshold (*t*-statistics = 4) shown by the right color bar. M indicates medial, and L indicates lateral. Right: Viral injection sites determined by the stimulation procedure in monkey Y. (d) cOFC microstimulation increased Av choices; conventions as in c. The size of increase in Av induced by stimulation at two sites in cOFC gray matter was significantly larger than that in the white matter (*P = 0.038, **P = 0.00008.4). Middle: Striatal fMRI signal induced by ipsilateral cOFC stimulation in monkey N.

FIGURE 2. pACC projections to striosomes. (a) Ipsilateral pACC projections in monkey S. pACC projection (hrGFP, green, left), KChIP1-positive striosomes (red, middle) and merged images (right), with enlarged views of the anterior striatum (framed by dashed line) at bottom. Asterisks indicate the same positions. AP positions in mm are based on the brain atlas for rhesus monkeys by Paxinos et al. (2000). Left is lateral, and right is medial. (b) Quantification of pACC projections to striatum calculated from the images of monkeys S, A, Y and N. Tracer densities (crosses) are

represented by normalized gray value of each striatal region (Materials and Methods). The normalized gray values were calculated separately for striosomes and matrix, and for anterior (n = 7, 8, 10 and 8 for ipsilateral, respectively, in monkeys S, Y, A and N; n = 10, 9 and 11 for contralateral, respectively, in monkeys Y, A and N), central (n = 9, 9, 9 and 10 for ipsilateral, respectively, in monkeys S, Y, A and N; n = 9, 9 and 9 for contralateral, respectively, in monkeys Y, A and N) and posterior (n = 9, 9, 8 and 11 for ipsilateral, respectively, in monkeys S, Y, A and N; n = 8, 9 and 9 for contralateral, respectively, in monkeys Y, A and N) regions. Figure S7 shows the details for each monkey. Red bars, means. Pink bars, SEM. Tracer densities were significantly greater in striosomes than in matrix in both hemispheres (paired *t*-test, $*P < 0.05$). (c) Effective microstimulation and viral injection sites (stars) in monkeys S (red), P (purple) and Y (blue), and stimulation site (square) in monkey N during fMRI (orange), mapped onto a sagittal drawing of a monkey's left side brain. Colored regions show the extent of viral injection sites (S, red; Y, blue; A, green; N, yellow).

FIGURE 3. cOFC projections to striosomes. Conventions as in Figure 2. (a) Ipsilateral cOFC projection (mCherry, red, left), KChIP1-positive striosomes (green, middle) and merged images (right) in monkey A. Right is lateral, and left is medial. (b) Quantification of pACC projections to the striatum calculated from the images of monkeys A and N. cOFC projections to striosomes were significantly different from those to matrix ($*P < 0.05$, $**P < 0.01$). The normalized gray value for striosomes and matrix was calculated for anterior (n = 10 and 8 for ipsilateral, n = 8 and 11 for contralateral, respectively in monkeys A and N), central (n = 9 and 10 for ipsilateral, n = 9 and 9 for contralateral, respectively in monkeys A and N) and posterior (n = 8 and 11 for ipsilateral; n = 9 and 9 for contralateral, respectively in monkeys A and N) regions. See the

details for each monkey in Figure S8. (c) Effective microstimulation sites and extents of viral injection sites mapped onto an orbital view of a monkey's left side brain.

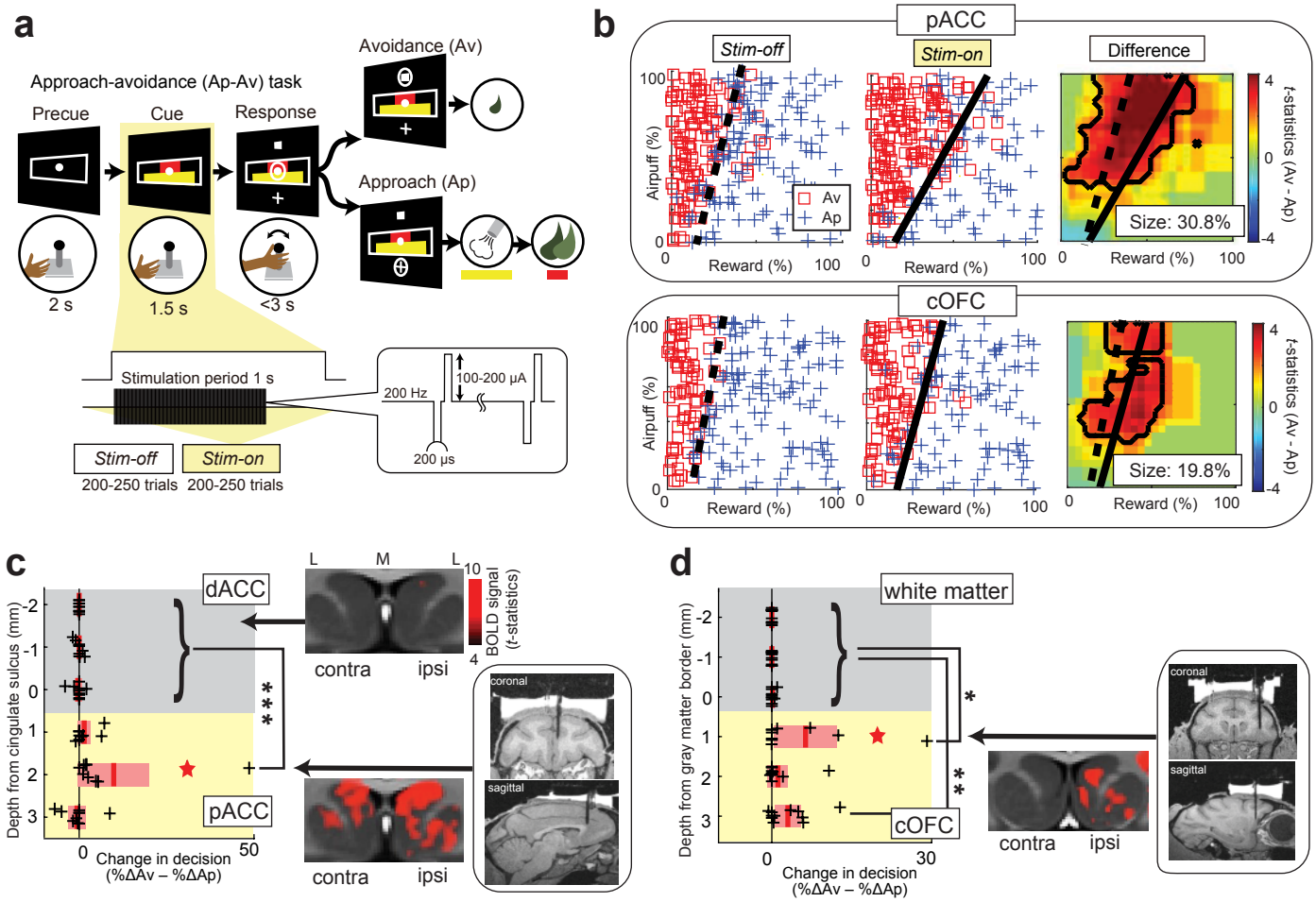
a
Approach-avoidance (Ap-Av) task
Precue
Cue
Response
Avoidance (Av)
Approach (Ap)
2 s
1.5 s
<3 s
Stimulation period 1 s
200 Hz
100-200 µA
200 µs
Stim-off
Stim-on
200-250 trials
200-250 trials
b
pACC
Stim-off
Stim-on
Difference
Airpuff (%)
Reward (%)
Av
Ap
Size: 30.8%
t-statistics (Av - Ap)
cOFC
Size: 19.8%
c
dACC
pACC
Depth from cingulate sulcus (mm)
Change in decision (%ΔAv – %ΔAp)
BOLD signal (t-statistics)
contra
ipsi
coronal
sagittal
d
white matter
cOFC
Depth from gray matter border (mm)
Change in decision (%ΔAv – %ΔAp)
contra
ipsi
coronal
sagittal

Figure 1

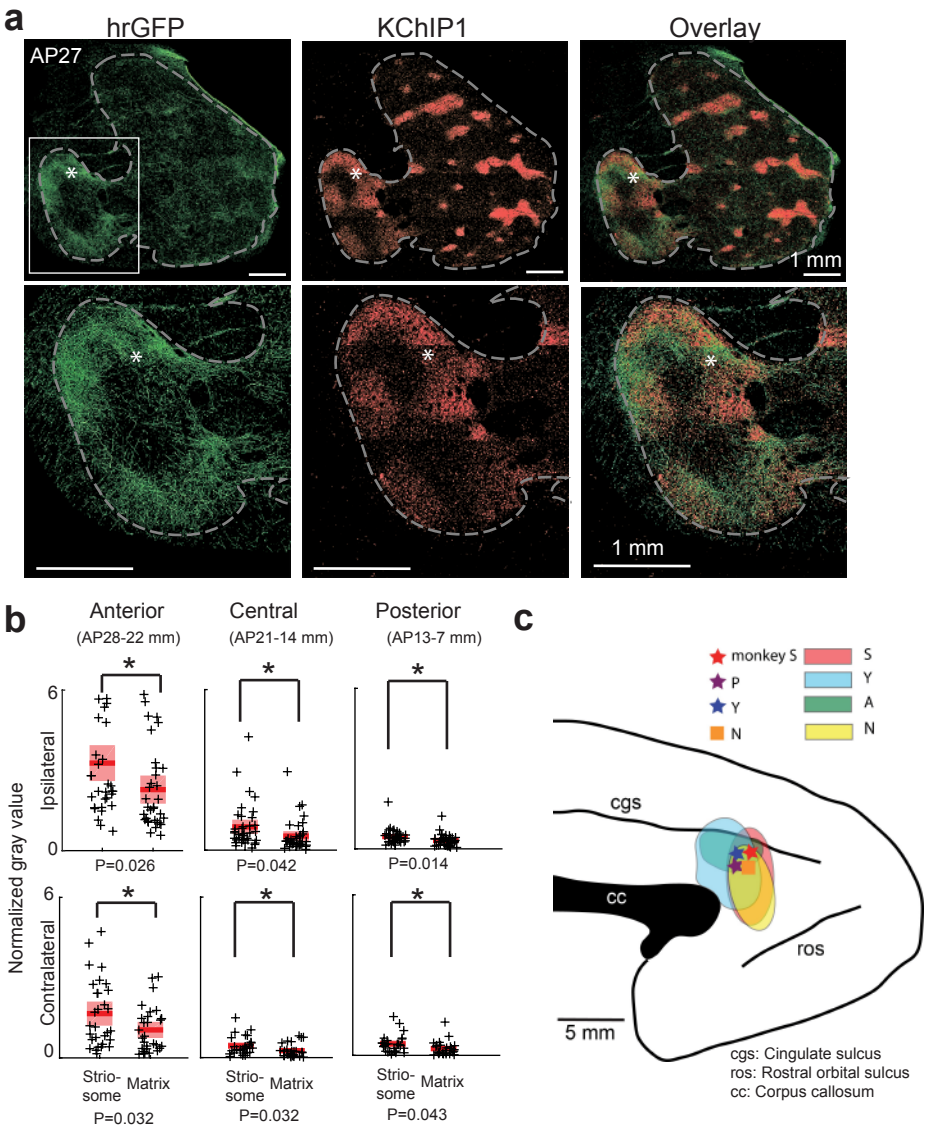
a
hrGFP
KChIP1
Overlay
AP27
1 mm
1 mm
b
Anterior
(AP28-22 mm)
Central
(AP21-14 mm)
Posterior
(AP13-7 mm)
Normalized gray value
Ipsilateral
Contralateral
6
0
P=0.026
P=0.042
P=0.014
Strio-some
Matrix
P=0.032
P=0.032
P=0.043
c
monkey S
P
Y
N
S
Y
A
N
cgs
cc
ros
5 mm
cgs: Cingulate sulcus
ros: Rostral orbital sulcus
cc: Corpus callosum

Figure 2

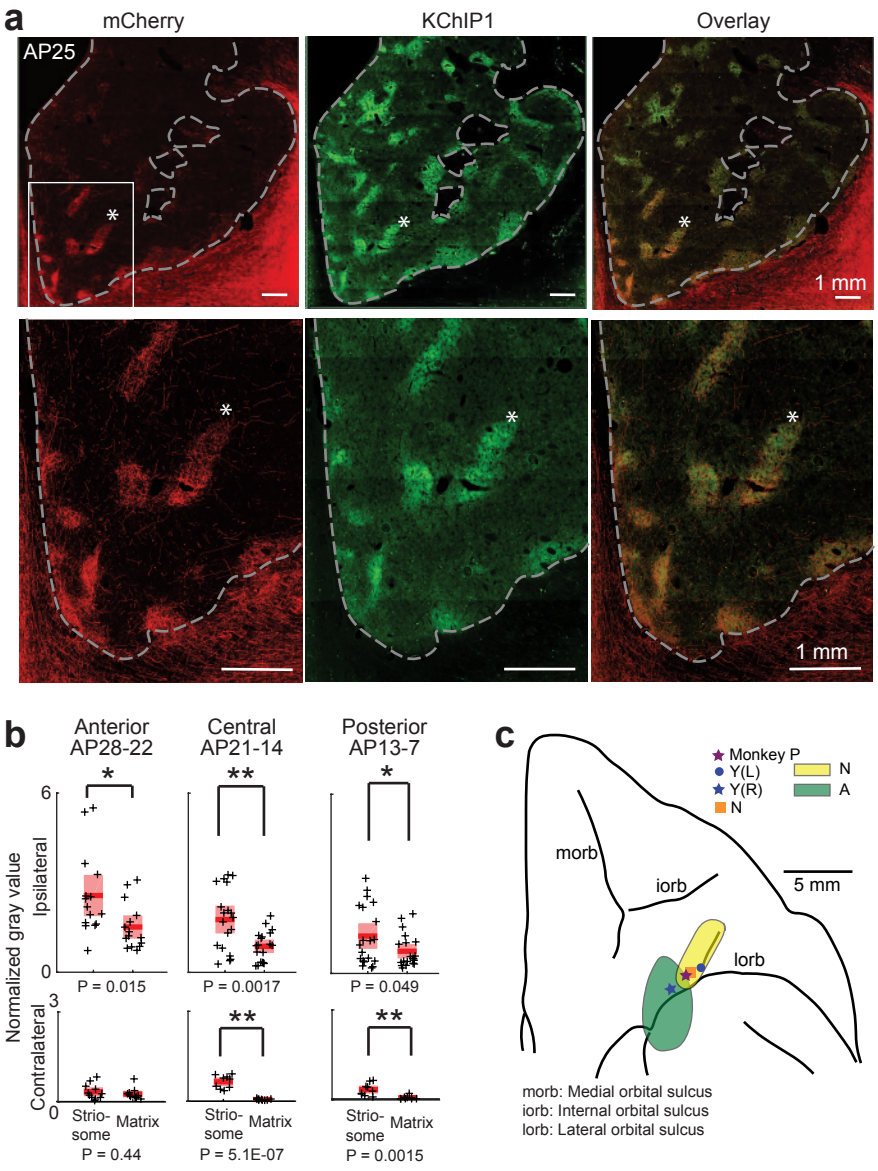
a
mCherry
KChIP1
Overlay
AP25
1 mm
1 mm
b
Anterior
AP28-22
Central
AP21-14
Posterior
AP13-7
Normalized gray value
Ipsilateral
Contralateral
P = 0.015
P = 0.0017
P = 0.049
P = 0.44
P = 5.1E-07
P = 0.0015
Strio-some
Matrix
c
Monkey P
Y(L)
Y(R)
N
N
A
morb
iorb
lorb
5 mm
morb: Medial orbital sulcus
iorb: Internal orbital sulcus
lorb: Lateral orbital sulcus

Figure 3

TABLE 1. Summary of monkeys used in this study and the experimental procedures applied to each monkey. L: left hemisphere, R: right hemisphere. F: female, M: male. Data from the left hemisphere of monkey Y with cOFC injection were not included due to the leakage of virus tracer to other cortical regions.

Monkey name (sex)	Stimulation during ApAv	Recording during ApAv	fMRI with stimulation	Virus injection (total amount)
Monkey S (F)	L & R pACC	R pACC	No	AAVDJ-CMV-hrGFP in LpACC (0.9 µl)
Monkey P (F)	LpACC, and LcOFC	LpACC, and LcOFC	No	No
Monkey A (F)	No	No	No	AAVDJ-CMV-hrGFP in RpACC (1.5 µl) AAVDJ-CMV-mCherry in RcOFC (1 µl)
Monkey Y (F)	RpACC, and L & R cOFC	No	No	AAVDJ-CMV-mCherry in RpACC (2 µl) *AAVDJ-CMV-hrGFP in LcOFC (1.4 µl) *Data not included
Monkey N (M)	No	No	RpACC, and RcOFC	AAVDJ-CMV-mCherry in RpACC (1 µl) AAVDJ-CMV-hrGFP in RcOFC (0.9 µl)
Monkey I (M)	No	No	No	AAVDJ-CMV-mCherry in LvCMA (1.4 µl)

Supporting Information

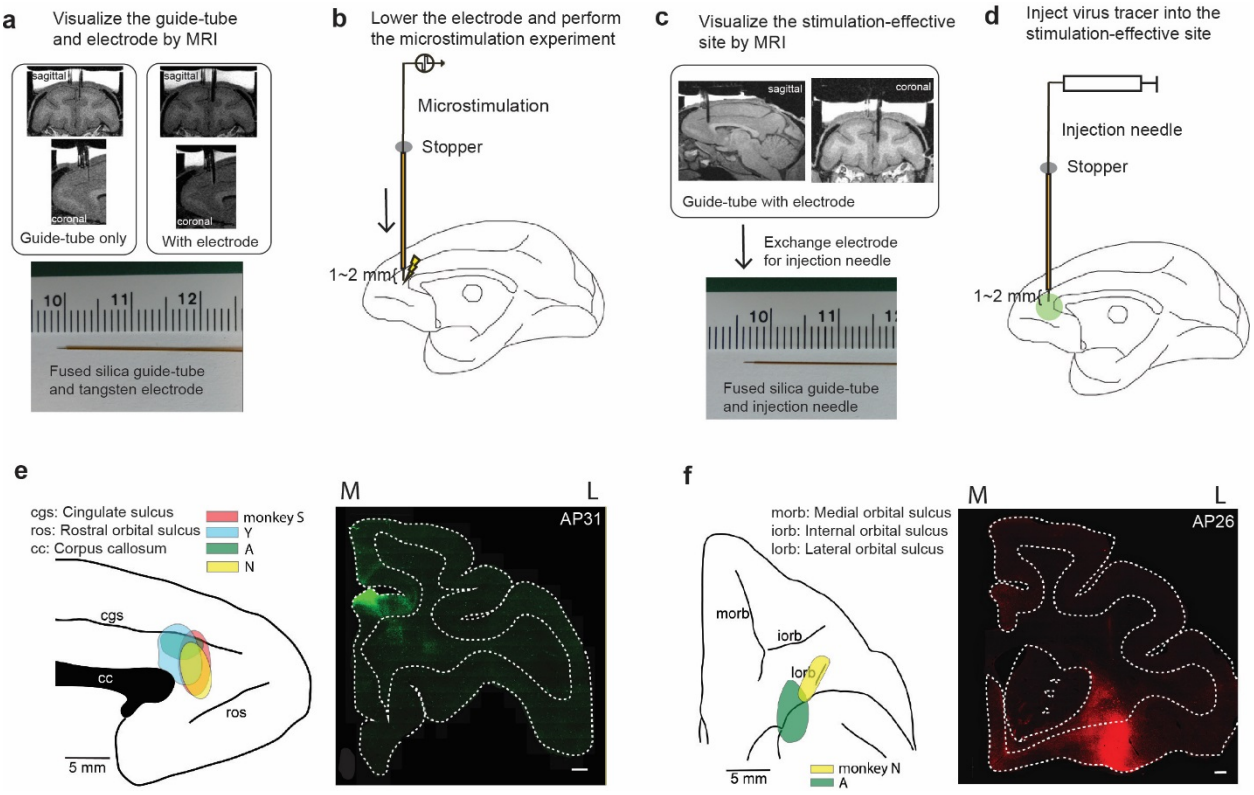

FIGURE S1. Experimental design to deliver microstimulation and infuse virus tracers at the same target cortical site. (a) We visualized the fused-silica guide tube lowered to the dACC region by MRI (top left panel). Then, we inserted a stimulation electrode through the guide tube until the stopper attached to the electrode prevented further lowering (top right panel). As we had already measured the distance between the tip of the electrode and that of the guide tube (bottom panel, 1-2 mm), we could estimate the position of the electrode tip and also estimate the artifact around the tip to be minimal (~1 mm). MRI images came from monkey Y. (b) We lowered the guide tube and electrode, and performed the microstimulation experiment to map out the function of each zone in the dACC and pACC (Figure 1b). We moved the guide tube and electrode every session toward the ventral part. (c) After functional mapping, we moved the electrode tip to the effective site and again visually identified the site by the MRI with the electrode (top panel and Figure 1c). To infuse the tracer virus, we left the guide tube and replaced the stimulation electrode with an injection needle. We had already put the stopper on the needle so that the needle tip would end up at the exact location where the electrode tip was (bottom panel). (d) We infused the tracer virus to the stimulation-effective site via the needle inserted into the guide tube. For the cOFC, we predetermined the infusion site in two monkeys (A and N) based on the results of other monkeys (P and Y), but we later confirmed that they were at the corresponding sites by performing histology (Figure 3c). (e and f) Schematic diagram (left) and representative images (right, monkey A) of tracer injection sites in pACC (e) and cOFC (f). Each color represents each monkey (red: S, blue: Y, green: A, yellow: N). Scale bars in images represent 1 mm. M indicates medial, L indicates lateral.

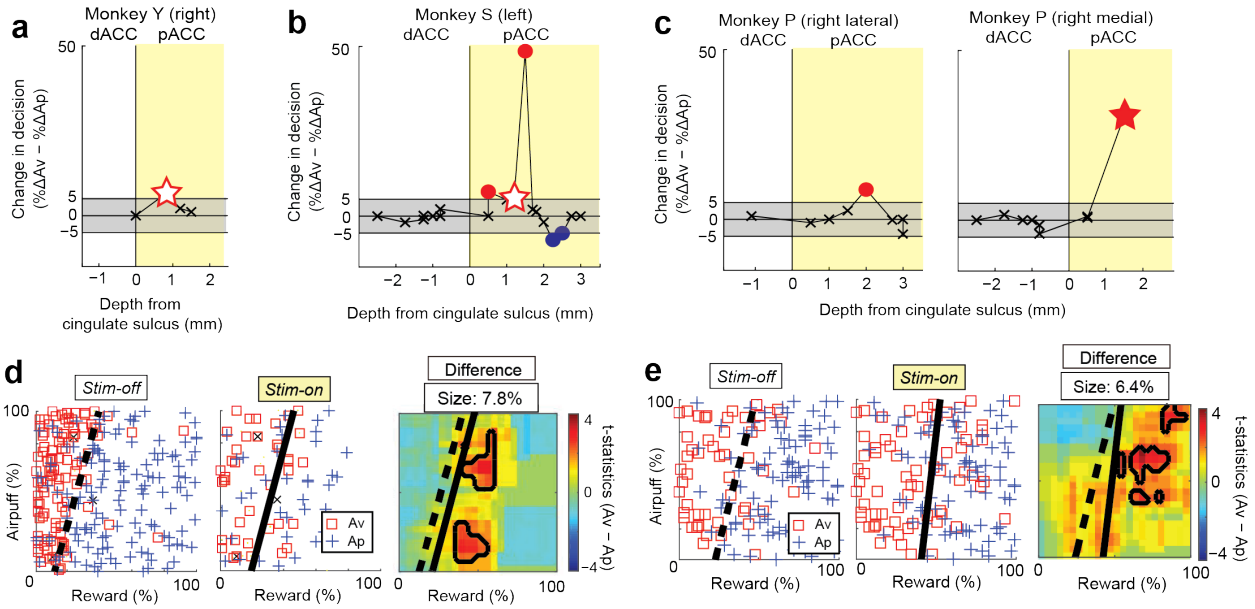

FIGURE S2. Microstimulation of the pACC, but not of the dACC, increased avoidance choices in all of three monkeys. (a-c) Changes in decision frequencies (%ΔAv − %ΔAp) by microstimulation in monkeys Y (a), S (b) and P (c), plotted against the depths from the cingulate sulcus. White stars indicate the virus infusion sites where we observed significant increases in Av choices in monkeys Y and S, shown in d and e, respectively. A red star shows the site where stimulation induced significant changes in decision in monkey P (shown in Figure 1b) but the tracer virus was not injected. We set a change of 5% as the significance level of the difference in decision matrix between the *Stim-off* and *Stim-on* blocks (see Materials and Methods). In each plot, crosses indicate changes below 5%. Red and blue circles indicate the sites where we observed significant increases in the Av and the Ap choices, respectively. (d and e) Changes in decision frequencies induced by microstimulation at the virus infusion sites in monkeys Y (d) and S (e), with decision matrices (see Materials and Methods) before stimulation (*Stim-off* block, left) and during stimulation (*Stim-on* block, middle), and smoothed differences in decision matrices between *Stim-on* and *Stim-off* blocks (right). Blue crosses indicate Ap choices, and squares indicate Av choices. Dashed and solid lines represent the decision boundary determined by the logistic regression for the *Stim-off* and *Stim-on* blocks, respectively.

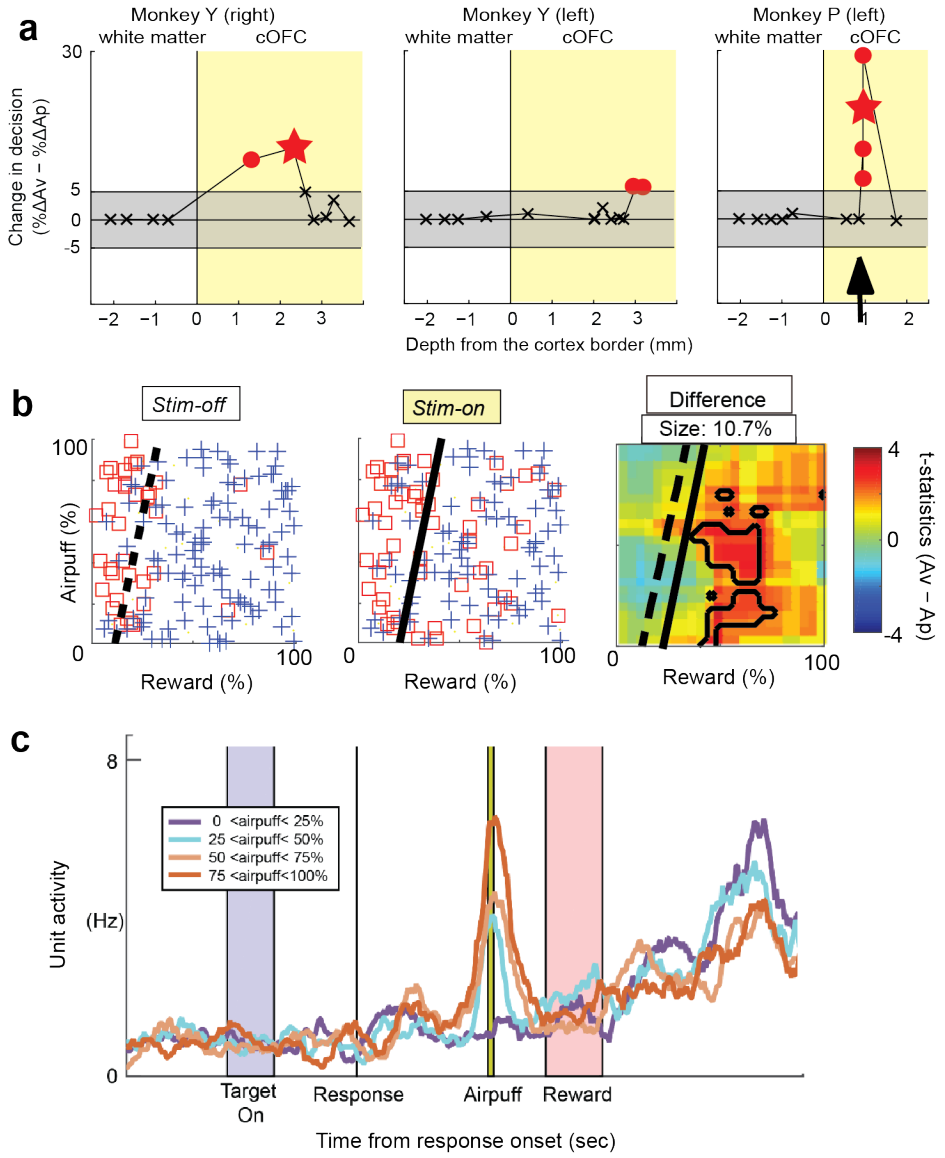

FIGURE S3. Microstimulation of the cOFC, but not surrounding sites, increased Av choices in two monkeys. (a) Changes in decision frequencies (%ΔAv − %ΔAp) by microstimulation in monkeys Y (left and middle panels) and P (right panel), plotted against the depths from the border between white and gray matters. Changes in decision in monkeys Y and P (red stars) are shown in b and Figure 1b, respectively. (b) Example of the effective stimulation observed in monkey Y (red star in a), shown as in Figure S2d. (c) A cOFC unit that encoded the delivery of an aversive stimulus. This unit was recorded at the site where microstimulation increased Av decisions in monkey P (arrow in **a**). The unit increased its firing rate, expecting delivery of the aversive stimulus (airpuff), and the magnitude of the increase depended on the strength of the airpuff.

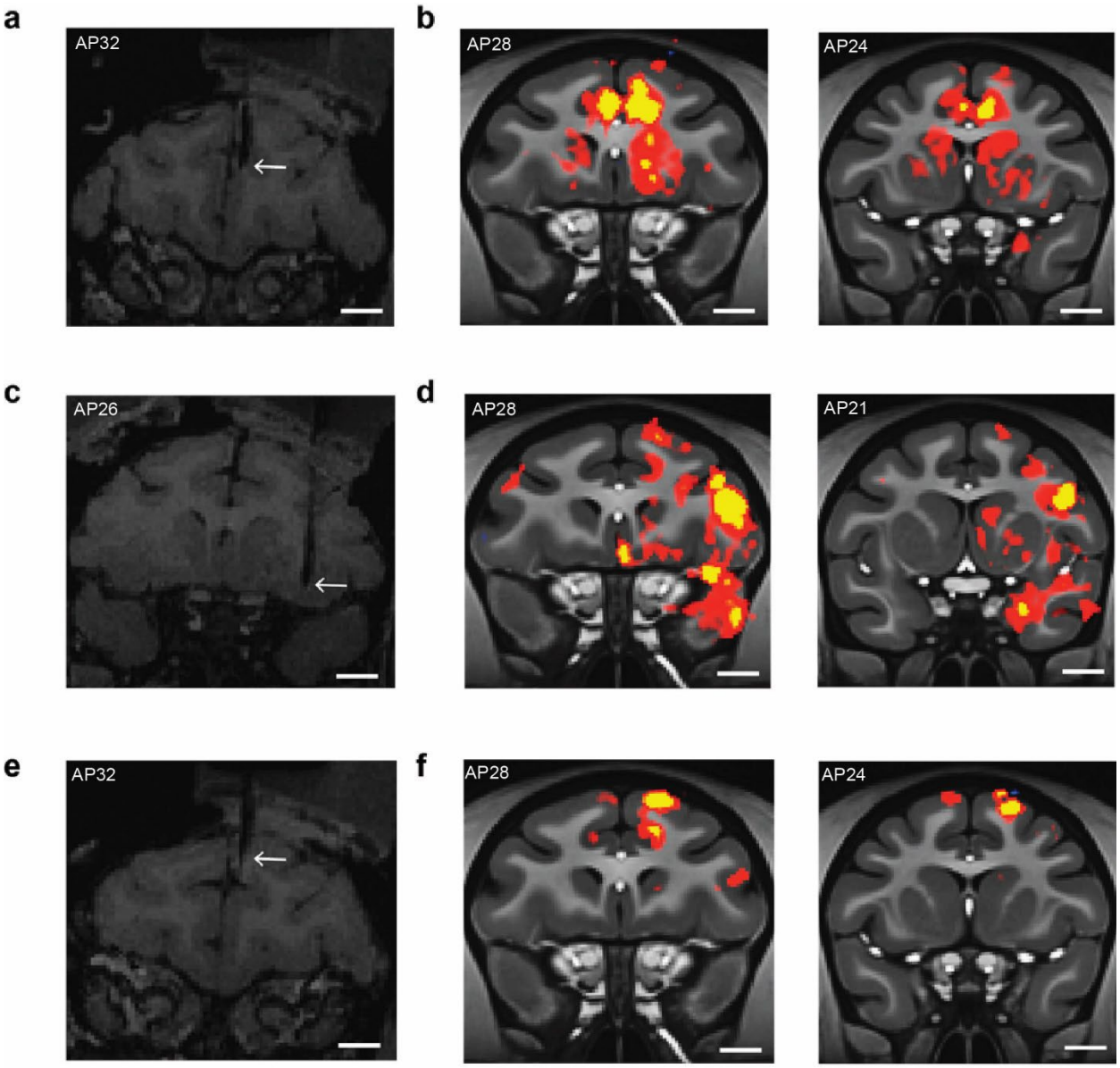

FIGURE S4. Microstimulation of the pACC and cOFC induced striatal activation visualized by fMRI. (a) Location of the stimulation electrode in the pACC (arrow) visualized by MRI in monkey N. (b) Strong activation induced by pACC microstimulation was detected in the anterior striatum by fMRI. Note that the activation was seen in both hemispheres and was stronger in the anterior to central region, consistent with the histology results. (c) Location of the stimulation electrode in the cOFC (arrow) visualized by MRI in monkey N. (d) Strong activation was induced by cOFC microstimulation in the anterior-to-central striatum. Note that the activation was seen only in the right (ipsilateral) hemisphere, in agreement with histology results. (e) Location of the stimulation electrode in the dorsal ACC (dACC, arrow) visualized by MRI in monkey N. This was a control location for the pACC. The electrode track was the same as the pACC, but the tip was located above the cingulate sulcus. (f) No activation was found in the striatum following dACC microstimulation. Scale bars represent 5 mm.

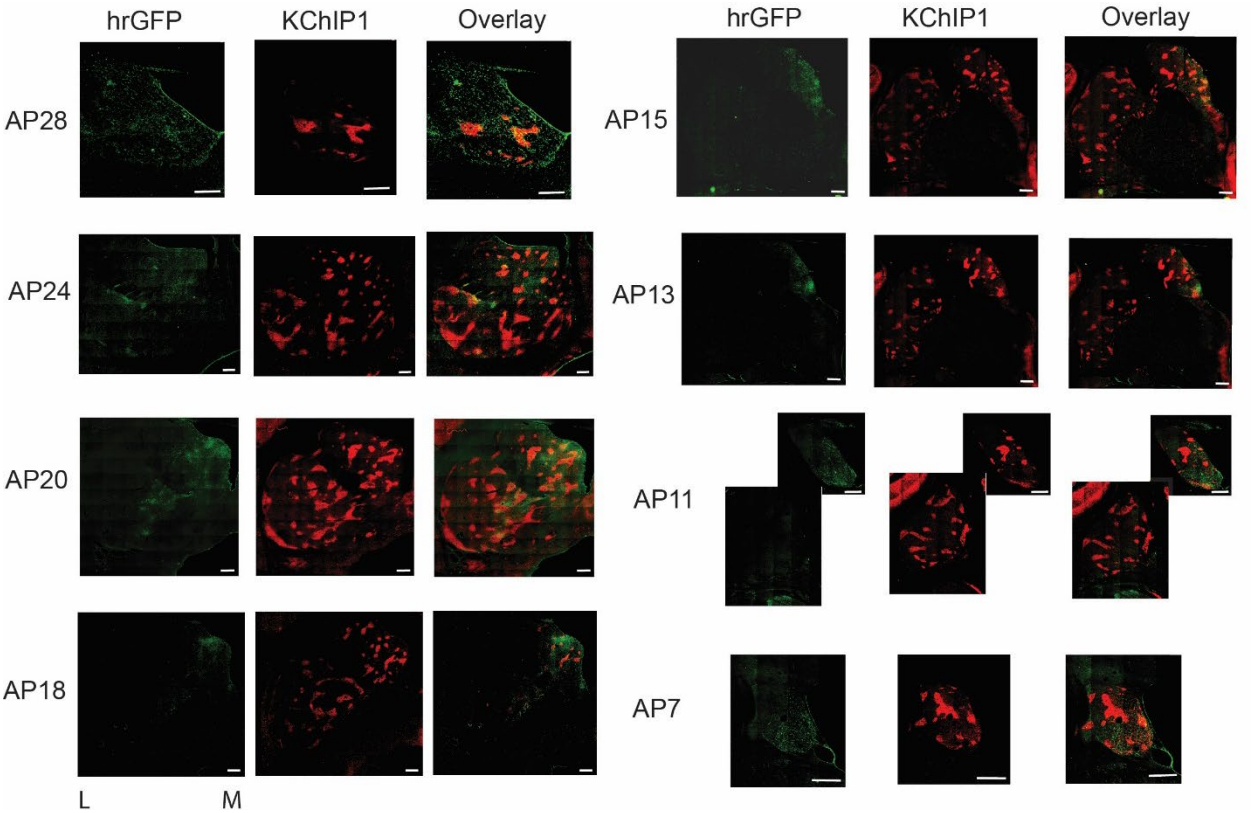

FIGURE S5. The pACC projects preferentially to ipsilateral striosomes. Representative images of left striatal sections from monkey S. These sections were double-stained for hrGFP (virus tracer, left) and KChIP1 (striosome marker, middle). Images at right show the overlay of hrGFP and KChIP1 images. Scale bars represent 1 mm. M indicates medial, and L indicates lateral. Anterior-Posterior (AP) position in mm referred to the brain atlas for rhesus monkeys (Paxinos et al., 2000)

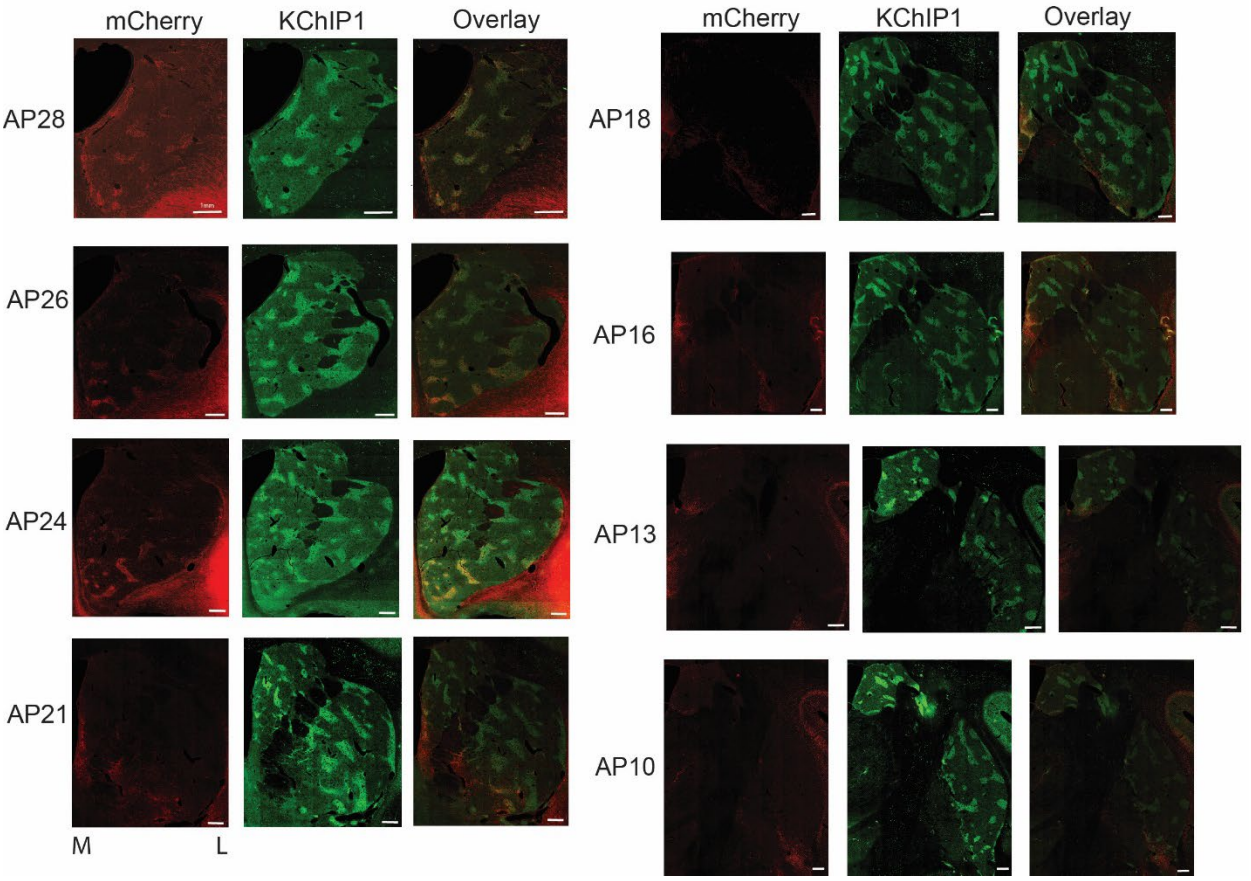

FIGURE S6. The cOFC projects preferentially to ipsilateral striosomes. Conventions as in Figure S5. Representative images of right striatal sections from monkey A. These sections were double-stained for mCherry (virus tracer, left) and KChIP1 (striosome marker, middle). Right images show the overlay of mCherry and KChIP1 images.

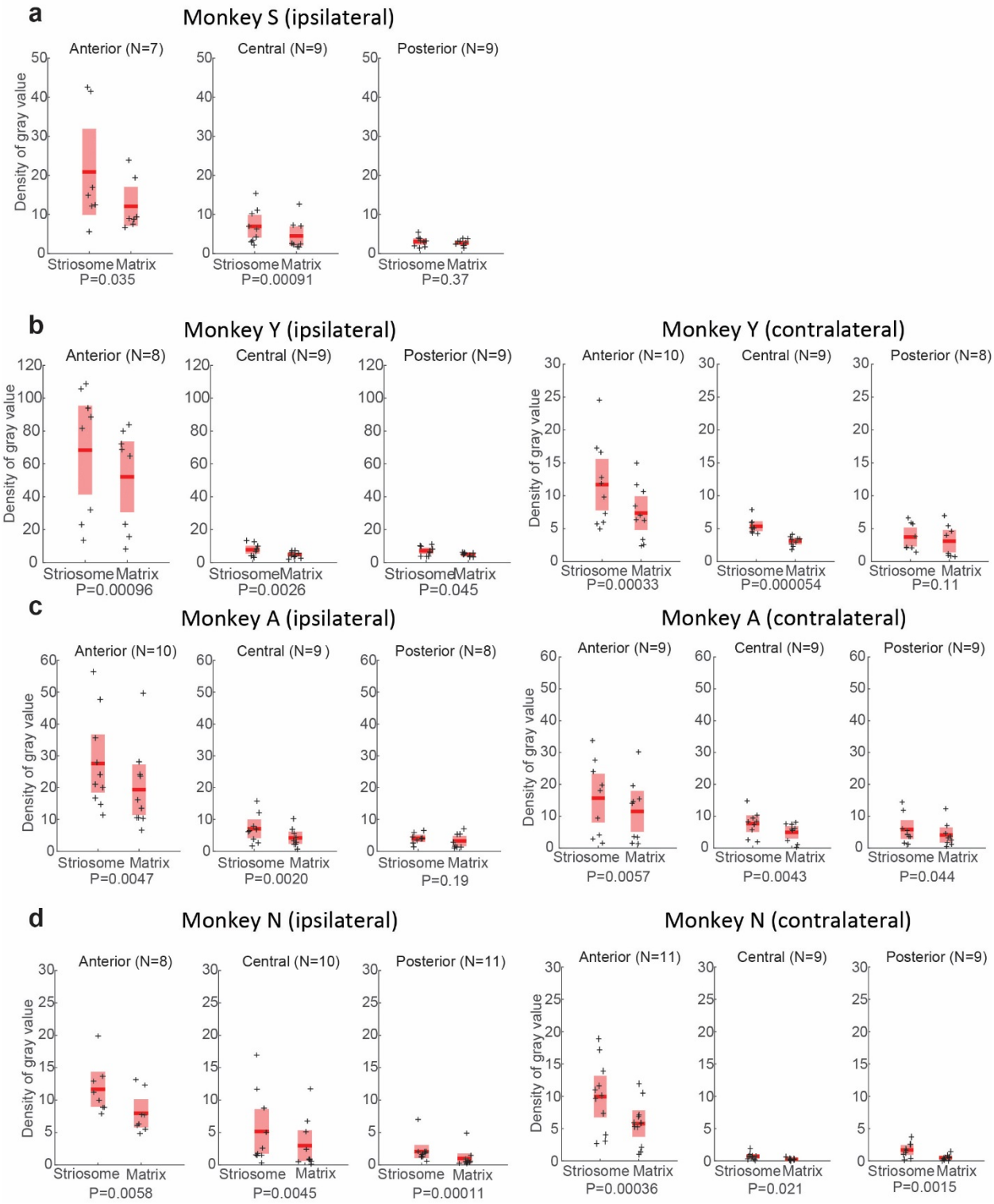

FIGURE S7. Summary of pACC projections to ipsilateral and contralateral striatum. Density of projections from the pACC to ipsilateral (left panels) and contralateral (right panels) striatum in monkeys S (a), Y (b), A (c) and N (d). Both ipsilateral and contralateral projections were more dense in the anterior part than in the posterior part. However, the overall density was smaller for contralateral projections compared to that for ipsilateral projections. For both ipsilateral and

contralateral striatum, pACC projections to striosomes were significantly denser than those to matrix in anterior and middle regions. Gray values (fiber density) were calculated from fluorescent images of histological sections (Materials and Methods), and striatal sections were classified into anterior (AP28-22), central (AP21-14) and posterior (AP13-7) regions. Error bars represent the standard error of the mean. The number of sections (N) and the results of paired t-tests (P) are indicated for each plot.

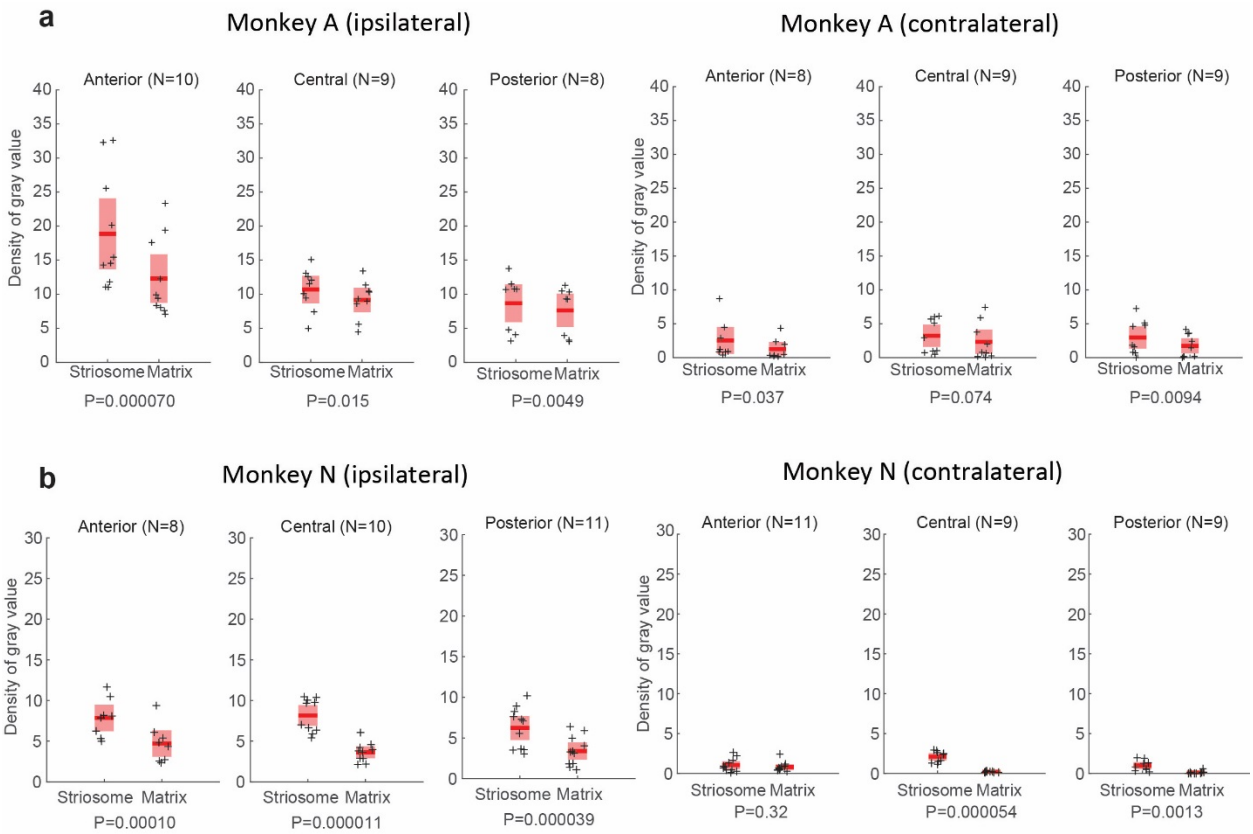

FIGURE S8. Summary of cOFC projects to ipsilateral and contralateral striatum. Density of cOFC projections to ipsilateral (right hemisphere) striatum in monkeys A (a) and N (b), shown as in Figure S7. The cOFC projections to ipsilateral striosomes were significantly greater than those to matrix in all regions in monkey A. Contralateral projections were weak in both monkeys.

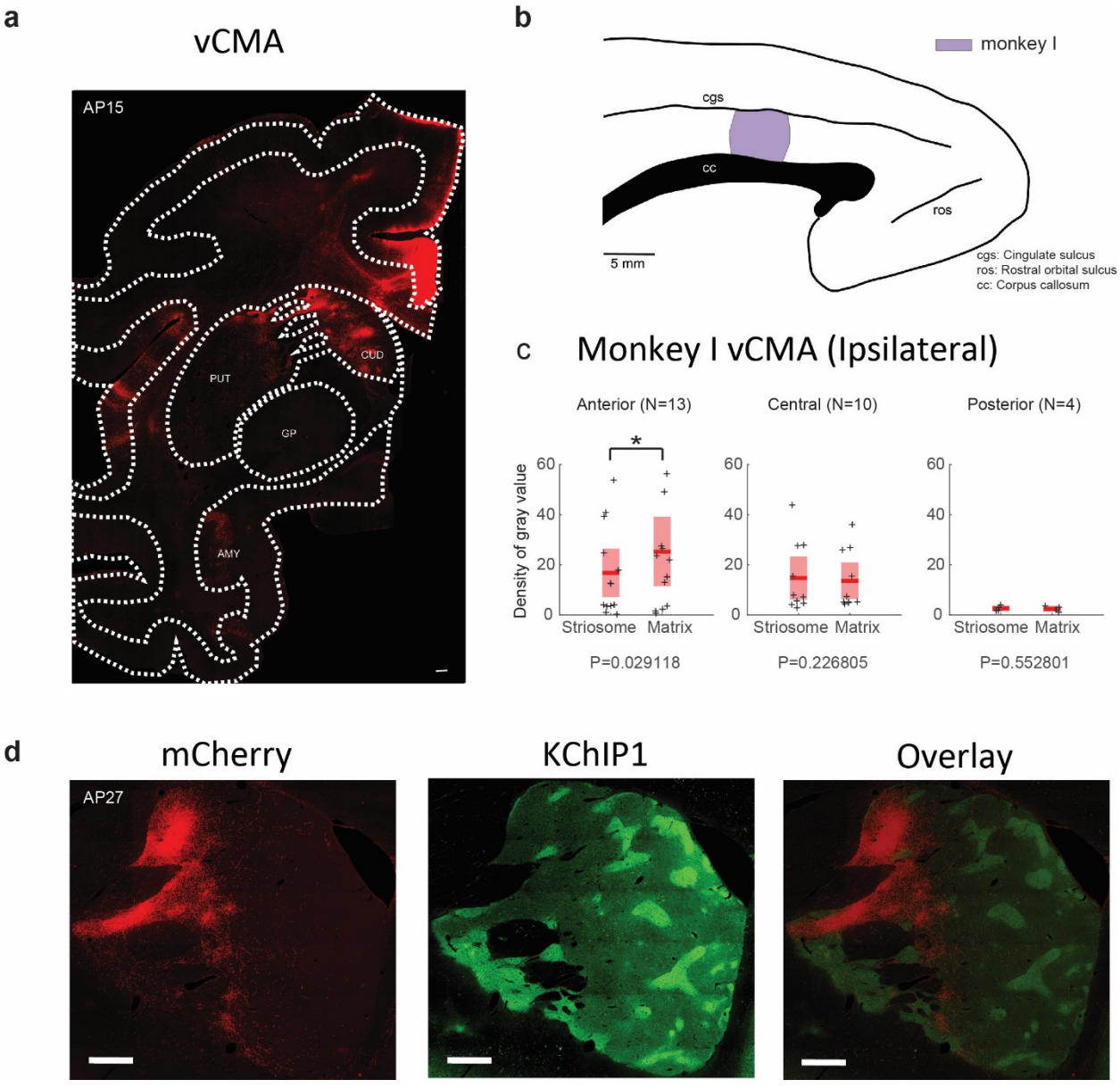

FIGURE S9. Summary of projections from the ventral cingulate motor area (vCMA) to ipsilateral matrix. (a) A sample image of the vCMA injection site in monkey I, stained for mCherry (red). CUD: Caudate, PUT: Putamen, GP: Globus Pallidus, AMY: Amygdala. (b) Schematic illustration of tracer injection sites (purple), shown in medial views of the left hemisphere. (c) Summary of vCMA projections to ipsilateral (left hemisphere) striatum in monkey I. Projections to ipsilateral matrix were significantly greater than those to striosomes in the anterior region. (d) Images of the anterior striatum section of monkey I, shown as in Figure S6. Scale bars represent 1 mm.